Microchimica Acta (2020) 187: 56
https://doi.org/10.1007/s00604-019-4057-6

ORIGINAL PAPER

Aggregation-based determination of mercury(II) using DNA-modified single gold nanoparticle, T-Hg(II)-T interaction, and single-particle ICP-MS

Yuqian Xing[1] · Juan Han[1] · Xu Wu[1] · David T. Pierce[1] · Julia Xiaojun Zhao[1]

Received: 11 June 2019 / Accepted: 28 November 2019 / Published online: 17 December 2019

Abstract

An ultrasensitive assay is described for the detection and determination of Hg^{2+}(aq) in water samples based on single-particle inductively-coupled plasma/mass spectrometry (spICP-MS). In the presence of Hg^{2+}(aq), AuNPs modified with a segment of single-stranded DNA aggregate due to the formation of the well-known thymine (T)-Hg^{2+}-T complex. Single particle (sp) ICP-MS is used quantify the degree of aggregation by the overall decrease in number of detected AuNPs or NP aggregates. Compared with most other Hg^{2+} assays that use the same principle of aggregation-dispersion with DNA modified AuNPs, this method has a much lower detection limit of (0.031 ng L^{-1}, 155 fM) and a wider (10,000-fold) linear range (up to 1 μg L^{-1}). The method also showed good practical potential because of its minimal interference from the water sample matrix.

Keywords Ionic mercury · Sub ng L^{-1} detection · Inductively coupled plasma mass spectrometry

Introduction

Mercury compounds are particularly hazardous pollutants because of their high toxicity and tendency to bio-accumulate, thereby causing serious risks to environmental and human health [1–3]. Mercury commonly exists in three basic forms: metallic or elemental mercury (Hg^0), ionic mercury (Hg^{2+} or Hg_2^{2+}) typically comprising sparingly soluble halide and chalcogenides compounds, and organic mercury like methylmercury [4]. The elemental mercury is volatilized during combustion of fossil fuels and is eventually oxidized to Hg^{2+} in the atmosphere and deposited on land or in the ocean [5]. This ionic mercury is easily methylated to organic mercury, which accumulates in the food chain to pose adverse health effects for human beings [6–9]. To establish safety margins for the food supply, the US Environmental Protection Agency (EPA) has set a maximum contaminant level for mercury in drinking water at 2.0 μg L^{-1}, and the US Food and Drug Administration (FDA) has set a safety threshold for mercury compounds in food at no higher than 1.0 mg L^{-1} [10, 11]. Therefore, it is essential to have sensitive and selective methods for monitoring low concentrations of Hg^{2+} in the environment and in food. EPA-approved methods with detection limits for ionic mercury include cold-vapor atomic absorption (Method 245.2, 5 ng L^{-1}) or atomic fluorescence (Method 245.7, 0.5 ng L^{-1}) spectroscopies and thermal decomposition, amalgamation, and atomic absorption spectrophotometry (Method 7473, 5 ng g^{-1}) [12]. Other published methods use molecular fluorescence spectroscopy [13, 14] or microextraction atomic absorption spectroscopy [15], but all are challenged or inadequate to detect ionic mercury levels below ng L^{-1}.

Nanomaterial-based methods and reagents are playing increasingly pivotal roles for trace level analysis (≤ mg L^{-1}) [16]. As a well-studied nanomaterial, gold nanoparticles (AuNPs) have been widely applied in various assays for Hg^{2+} based on their excellent optical, electrochemical and other properties [17–19]. As far as we know, previous studies

Yuqian Xing and Juan Han contributed equally to this work.

Electronic supplementary material The online version of this article (https://doi.org/10.1007/s00604-019-4057-6) contains supplementary material, which is available to authorized users.

✉ David T. Pierce
david.pierce@und.edu

✉ Julia Xiaojun Zhao
julia.zhao@und.edu

[1] Department of Chemistry, University of North Dakota, Grand Forks, ND 58202, USA

have focused exclusively on Hg^{2+} induced aggregation of AuNPs, which can be manifested by a significant change of the AuNP plasmon peak [18]. Two strategies are commonly used to conduct these assays. One is to disrupt the protecting function of the surface ligands of the AuNPs under special conditions, like high ionic strength conditions, thereby causing the aggregation of the AuNPs [20]. For instance, Liu and co-workers designed AuNPs with a physically adsorbed single-stranded DNA (ssDNA), that form double-stranded DNA (dsDNA) in the presence of Hg^{2+} due to the thymine-Hg^{2+}- thymine (T-Hg^{2+}-T) interaction [21]. The dsDNA easily desorb from the surface of the AuNPs and induce an aggregation at high NaCl concentrations that is proportional to Hg^{2+} concentration. Another strategy uses a Hg^{2+}-induced crosslinking reaction between two or more AuNPs modified with the same or different ligands, respectively. For example, Du and co-workers used urine to ligate the surface of AuNPs and work as ligands. Adding Hg^{2+} led to crosslinking of the AuNP ligand and induced the aggregation of AuNPs [22]. Despite the success of these methods at promoting Hg^{2+}-selective aggregation of AuNPs, their sensitivity is compromised by the finite absorptivity of the AuNP plasmon band [23, 24].

Over the last decade, single-particle inductively-coupled plasma/mass spectrometry(spICP-MS) has gained increasing research interest for nanomaterial analysis [25–27]. Such spICP-MS can provide not only information about the nanoparticle size and size distribution, but it can also directly determine the number of nanoparticles in solution. Furthermore, interactions such as agglomeration and disaggregation between two or more nanoparticles can be easily identified by changes to the spICP-MS signal. Combined with the excellent analytical characteristics of the ICP-MS [28], including high sensitivity, wide linear range, and absolute quantification, routine single-nanoparticle analysis is now a promising starting point for extremely sensitive environmental and bioassays. Because AuNPs are composed of a highly abundant isotope (^{197}Au) and are easy to functionalize, they are becoming widely applied in spICP-MS studies. For instance, Han and co-workers developed a one-step homogeneous DNA assay with AuNPs using spICP-MS. The concentration-dependent changes to the spICP-MS made it possible to detect target DNA down to 1 pM [29].

We present a new strategy for highly sensitive and selective determination of Hg^{2+} ion using spICP-MS of AuNPs modified with ssDNA. Samples of 30 nm AuNPs are individually functionalized with two ssDNA probes (Probe 1 and Probe 2). In the presence of Hg^{2+}, agglomeration occurs between AuNP-Probe 1 conjugates and AuNP-Probe 2 conjugates due to the formation of T-Hg^{2+}-T containing dsDNA. The reduced number of AuNPs or NP clusters observed by spICP-MS decreases with Hg^{2+} concentration in a well-defined manner, yielding an assay that can selectively detect Hg^{2+} as low as 0.031 ng L^{-1}.

Experimental

Chemicals and instruments

Gold nanoparticles with different sizes were purchased from Cytodiagnostics Inc. (Burlington, Canada, http://www.cytodiagnostics.com). Mercury standard (AAS), mercury(II) chloride (ACS reagent), (11-mercaptoundecyl)hexa(ethylene glycol) (TOEG6, > 90%), tris(2-carboxyethyl)phosphine hydrochloride (TCEP, >= 98%), polyethylene glycol sorbitan monolaurate (Tween-20, GC, >= 40%), sodium chloride (99.5%), sodium phosphate monobasic (99.0%), sodium phosphate dibasic (99.0%), sodium citrate tribasic dihydrate (99.0%), tris-borate-EDTA (TBE) buffer (5× concentrate), agarose (for molecular biology) were purchased from Sigma-Aldrich (St. Louis, MO, www.sigmaaldrich.com). A mercury certified reference material used for method validation, SRM1641e (Mercury in Water), was obtained from the National Institute of Standards & Technology (Gaithersburg, MD, https://www.nist.gov/). Deionized (DI) water (18.2 MΩ•cm) was produced from a Millipore water purification system. The following DNA sequences were synthesized by Integrated DNA Technology (Coralville, IA, https://www.idtdna.com) and used as received.

Probe 1 (A_{10}P1): 5′-HS-$(CH_2)_6$-A_{10}-GGTTGTGT TCGTGTGC-3′
Probe 2 (A_{10}P2): 5′-HS-$(CH_2)_6$-A_{10}-GCTCTCGT TCTCTTCC-3′

Water samples used for method validation were collected without headspace in EPA performance-standard 250 mL HDPE containers (Thermo Scientific, www.thermofisher.com), acidified with 1.5 mL of 1:1 diluted Optima-grade concentrated nitric acid (Fischer Chemical, www.fishersci.com), and stored for less than 28 days under refrigeration (8 °C). Tap water (Grand Forks, ND) was draw from a laboratory sink and river water (Red River of the North) was drawn directly from a settling tank at the Grand Forks water treatment plant.

Instruments

UV-Vis absorption measurements were performed with a PerkinElmer Lambda 1050 UV/Vis/NIR spectrometer (PerkinElmer, Santa Clara, CA), equipped with a Peltier temperature control accessory. Transmission electron microscopy (TEM) images of ssDNA modified AuNPs were acquired by

Hitachi 7500 transmission electron microscope (Hitachi, Japan).

A ThermoFisher iCAP Q ICP-MS (Waltham, MA, U.S.A) equipped with a microflow perfluoroalkoxy nebulizer and a quartz cyclonic spray chamber cooled to 2.70 °C, was used to monitor the ICP-MS signals of AuNPs. The sample solution was introduced into the ICP-MS using a peristaltic pump operating at 20 rpm and with PVC peristaltic pump tubing of 0.508 mm i.d (ThermoFisher, Waltham, MA, U.S.A) yielding a normal flow rate of 0.2 mL min^{-1}. The exact sample flow rate was measured daily by mass of DI water. The ICP-MS instrument was tuned daily using a multi-element solution (1 μg/L In, U, and Ce in 2.5% (*v*/v) HNO_3) for maximum ^{115}In, ^{238}U and minimum $^{140}Ce^{16}O/^{140}Ce$ level (<3.0%) under high-sensitivity standard mode. Additional ICP-MS instrument operating parameters are provided in Table S1. Integrated isotope ^{197}Au signals in counts were recorded with a dwell time of 5 ms over a total acquisition period of 180 s, thereby capturing 36,000 individual measurements per sample. Particle number and count intensities were derived throughout this work by making two important assumptions. (i) The isotope counts generated for one AuNP or NP cluster occurred entirely within one dwell time. (ii) No more than one AuNP or NP cluster was sampled per dwell time. The nanoparticle detection criterion used in this work was any measurement above 5 counts, which was five-times the background shot noise of the detector. Measurement evaluation was performed using Microsoft Excel and Origin (Northampton, Massachusetts, USA).

EPA method 7473 (Feb. 2007 Revision 0) for determination of mercury in solids and liquids was used as a comparison method to the spICP-MS assay for environmental samples. The method 7473 measurements were performed with a Milestone DMA-80 Tri Cell direct mercury analyzer (Shelton, CT) equipped with a 40-position auto-sampler. Liquid samples were weighed to 0.1 mg in quartz sample boats and placed on the auto-sampler spindle. Samples were individually dried and then decomposed under the flow of regulated oxygen carrier gas. An amalgamator was used to trap the elemental mercury after which the trap was rapidly heated and mercury vapor was carried sequentially through three quartz cells positioned in the light path of atomic absorption spectrophotometer. Transient absorbance of mercury was measured at 253.7 nm for each cell and related back to mercury concentration in the sample by external calibration over three ranges. Specific instrument operating parameters are listed in Table S2.

Preparation of ssDNA modified AuNPs

Thiol-functionalized ssDNA (SH-ssDNA) (100.0 μL of 200.0 μM) was first reduced in the same volume of TCEP (20.0 mM), and incubated for 2 h at room temperature. The amount of ssDNA was quantified with UV-Vis spectrometry. The modification of ssDNA onto AuNPs was performed according to the literature with a slight change [30]. Briefly, the reduced SH-ssDNA (10.0 μL of 100.0 μM) was mixed with 1 mL of 330 pM 30-nm-diameter AuNPs under vortexing for 1 min and left to rest for 30 min at room temperature. Afterward, an aliquot of 100.0 μL of 100 mM citrate-HCl buffer pH 4.3 was added to adjust the pH of the solution and incubated for another 30 min, followed by adding 10.0 μL of 300 μM TOEG6. After another 30 min static incubation, the solution was centrifuged at 6000 rpm for 30 min. The precipitates were collected and washed twice with DI water. The final pellet was re-dispersed in 1.0 mL of DI water and stored at 4 °C for further usage.

Method development

Several method conditions required optimization prior to calibration and validation. These conditions included the concentration of AuNP-DNA composites incubated with Hg^{2+} samples or standards, as well as the temperature and time of the incubation. The conditions were varied to optimize a dimensionless aggregation efficiency (γ, Eq. 1) calculated from the single-particle data acquired by the ICP-MS.

$$\gamma = 1 - \frac{\text{number of AuNPs detected } \textbf{after } Hg^{2+} \text{exposure}}{\text{number of AuNPs detected } \textbf{before } Hg^{2+} \text{exposure}} \quad (1)$$

Optimization of particle number concentration was conducted with ssDNA modified AuNPs (AuNP-A_{10}P1 and AuNP-A_{10}P2) serially diluted 1:10 from 10^{10} to 10^{6} particles (P) mL^{-1} with 10 mM pH 7.4 phosphate buffer (PB) containing 300 mM NaCl. Aliquots of 90 μL of AuNP-A_{10}P1 and 90 μL of AuNP-A_{10}P2 were mixed, followed by a 20 μL addition of Hg^{2+} solution of varied concentration. The mixture was subsequently heated up to 95 °C for 5 min, cooled to room temperature, and then incubated for 2 h with constant shaking to finish the reaction. An aliquot of 0.2 μL of Tween 20 was added and incubated in an ultrasonic water bath for another 5 mins before diluting to 5×10^4 P mL^{-1} of AuNPs and then performing spICP-MS measurements.

Subsequently, incubation temperature was varied between 20 to 40 °C and incubation time was varied between 30 min to 4 h to determine their optimum values.

Optimized method

The prepared ssDNA modified AuNPs (AuNPS-A10P1 and AuNPs-A10P2) were first diluted to 10^8 particles/mL (1.65 pM) with 10 mM pH 7.4 PB containing 300 mM NaCl. Aliquots of 90 μL of AuNP-A_{10}P1 and

90 μL of AuNP-A_{10}P2 were mixed, followed by a 20 μL addition of Hg^{2+} solution. Calibration solutions and NIST certified reference material (SRM1641e) samples were used directly following serial dilution, but mercury-spiked natural water samples (tap and river water) were pre-filtered to 0.45 μm. The mixture was subsequently heated up to 95 °C for 5 min, cooled to room temperature, and then incubated for 2 h with constant shaking to finish the reaction. An aliquot of 0.2 μL of Tween 20 was added and incubated in an ultrasonic water bath for another 5 mins before diluting to 5×10^4 P mL^{-1} of AuNPs and then performing spICP-MS measurements.

Results and discussion

This work established a new strategy (Scheme 1) for ultrasensitive and selective detection of Hg^{2+} ion by using spICP-MS to monitor the agglomeration of monodisperse AuNPs by T-Hg^{2+}-T paring of ssDNA on the AuNP surfaces. T-rich ssDNA probes (A_{10}P1 or A_{10}P2) are individually immobilized on separate AuNP samples. The two probes are complementary except for seven mismatched T bases. In the absence of Hg^{2+}, affinity between the two probes is too weak to cause binding at room temperature—a temperature much higher than their melting temperature. In the presence of Hg^{2+}, the T-Hg^{2+}-T interaction increases the melting temperature of dsDNA formed between two probes and causes aggregation for a portion of the AuNPs. Higher concentrations of Hg^{2+} increases the degree of aggregation, which is easily distinguished by spICP-MS measurements of ^{197}Au count intensity and number of individually detected particles or particle clusters.

Synthesis of AuNP-ssDNA

UV-Vis spectroscopy was used to confirm immobilization of ssDNA on AuNPs. Compared to bare AuNPs, the plasmon resonance peak of AuNPs modified with ssDNA (A_{10}P1 or A_{10}P2) is red-shifted to 530 nm from 526 nm (Fig. 1a). A new peak at 260 nm also demonstrates the immobilization. After addition of 10 mg L^{-1} Hg^{2+}, aggregation of DNA-modified AuNPs shows a significant red-shift and broadening of the UV-Vis plasmon peak (Fig. 1b). Successful immobilization of ssDNA on the AuNPs was also supported by gel electrophoresis, with which the movement of AuNPs can be visually tracked by their characteristic red color. As shown in Fig. 1c, AuNPs modified with ssDNA (lanes 2–4) move at a relatively fast speed that is aided by the negatively charged ssDNA. Bare AuNPs in lane 1 move more slowly than the modified AuNPs. The AuNP-ssDNA sample aggregated by Hg^{2+} in lane 5 shows a tailed band and moves much more slowly than the bare AuNPs due to their increased size after aggregation.

The size and stability of AuNPs modified with ssDNA were also characterized by TEM. Monodispersed AuNPs with the size of 32 ± 5 nm are observed no matter which ssDNA probe is immobilized (Fig. 2a-c). Even in the mixture of AuNP-A_{10}P1 conjugate and AuNP-A_{10}P2 conjugate, the particles remain monodisperse in the absence of Hg^{2+} (Fig. 2d), indicating excellent selectivity of the aggregation process.

Method feasibility

Capacity of the spICP-MS to quantify the size and number of AuNPs was investigated. It was expected that aggregation of

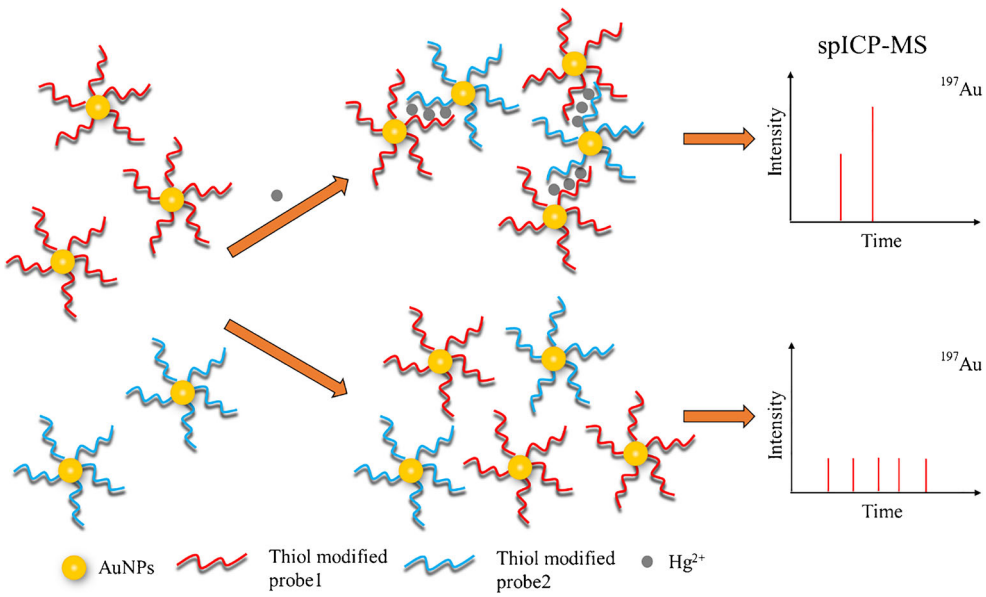

Scheme 1 Schematic illustration of Hg^{2+} determination by using modified AuNP probes measured by spICP-MS

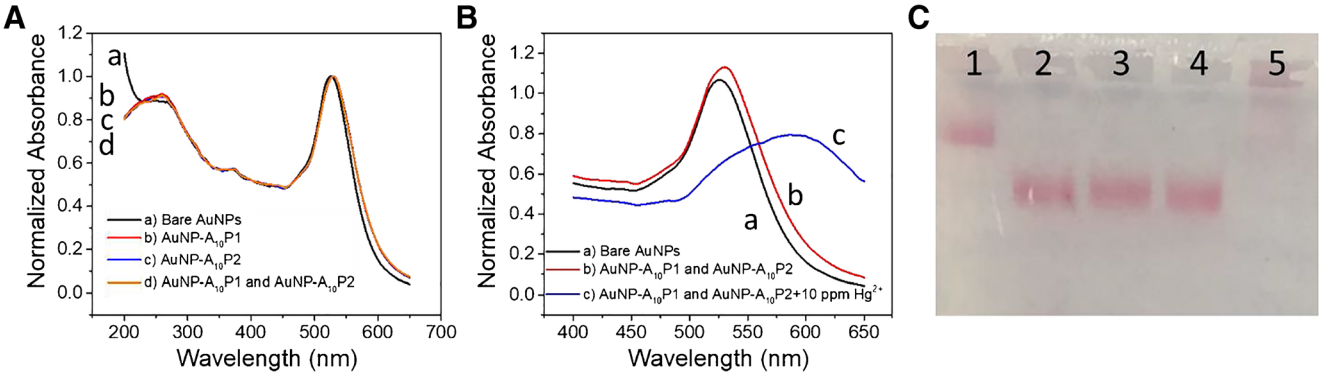

Fig. 1 Characterization of AuNP-ssDNA composites. **a**, UV-Vis spectra of bare and AuNPs modified with ssDNA; **b**, UV-Vis spectra of AuNP-ssDNA with or without 10 ppm Hg^{2+} in water; **c**, Electrophoresis gel image of AuNP-ssDNA: Lane 1 with bare AuNPs, Lane 2 with AuNP-A_{10}P1 conjugate, Lane 3 with AuNP-A_{10}P2 conjugate, Lane 4 with AuNP-A_{10}P1 conjugate and AuNP-A_{10}P2 conjugate, Lane 5 with AuNP-A_{10}P1 conjugate and AuNP-A_{10}P2 conjugate +10 mg L^{-1} of Hg^{2+}. Electrophoresis gel was performed using 1% agarose gel in 1× TBE buffer under 100 V for 20 min

AuNPs would decrease the number of detected nanoparticles within an acquisition period but increase the count intensity of some that were detected. To evaluate the instrument's ability detect these changes, AuNPs with different sizes and concentrations were analyzed (Figure S1). AuNPs of 20 nm, 30 nm, 40 nm, and 60 nm show peaks with average intensities increasing from 18.1 ± 0.8 to 450 ± 20 counts (Figure S1A-D). Plotting these average intensities versus the average AuNP mass (calculated from average diameter and density) shows a strong linear correlation over a wide range (Figure S2A) and demonstrates that changes in AuNP/cluster size caused by aggregation can be quantified by the spICP-MS. Samples of the same 30 nm AuNPs at incrementally higher concentrations from 1×10^4 to 1×10^5 P mL^{-1} also show increasing numbers of detected AuNPs during the same acquisition period (Figure S1 E-H). Plotting these numbers versus the particle concentration also shows a strong linear correlation over a wide range (Figure S2A) and likewise demonstrates that changes in particle number caused by aggregation can be quantified by the spICP-MS.

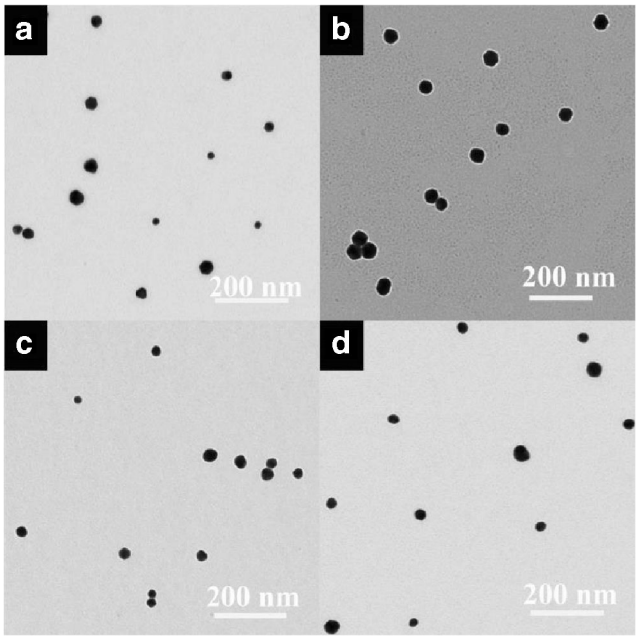

Fig. 2 TEM image of AuNPs modified with ssDNA. **a**, bare AuNPs; **b**, AuNP-A_{10}P1 conjugate; **c**, AuNP-A_{10}P2 conjugate; **d**, AuNP-A_{10}P1 conjugate and AuNP-A_{10}P2 conjugate

Another consideration for method feasibility is the capacity of the incubation medium to prevent aggregation when Hg^{2+} is not present (i.e., prevent false positives). Concentration of NaCl during incubation is known to affect binding affinity of Hg^{2+} and thymine group at moderate levels and to cause indiscriminate aggregation of AuNPs at high levels [31]. spICP-MS was used to evaluate saline stability of prepared AuNP-ssDNA, whether individually (AuNP-A_{10}P1 or AuNP-A_{10}P2) or as a mixture. Measured intensities recorded for modified AuNPs in PB (10 mM, pH 7.4) with 1 M NaCl (Figure S3 D-F), an NaCl concentration much higher than that used for the optimized binding buffer used in this work (300 mM), were identical to measured intensities with a saline-free PB (10 mM, pH 7.4) (Figure S3 A-C). No unusually high peaks were observed that might indicate aggregated AuNPs and the average number of AuNPs detected during the same acquisition period were also same to that in PB (10 mM, pH 7.4) without NaCl. These results demonstrate that the AuNP-ssDNA conjugates remain monodispersed in a relatively high concentration of NaCl.

Method optimizations

A dimensionless aggregation efficiency based on number of detected AuNP/clusters (γ, Eq. 1) was used to optimize key assay conditions and ultimately to calibrate the method. Although changes in both the number and average peak intensity AuNP/clusters detected within the acquisition period (180 s) can be used to evaluate the amount of aggregation,

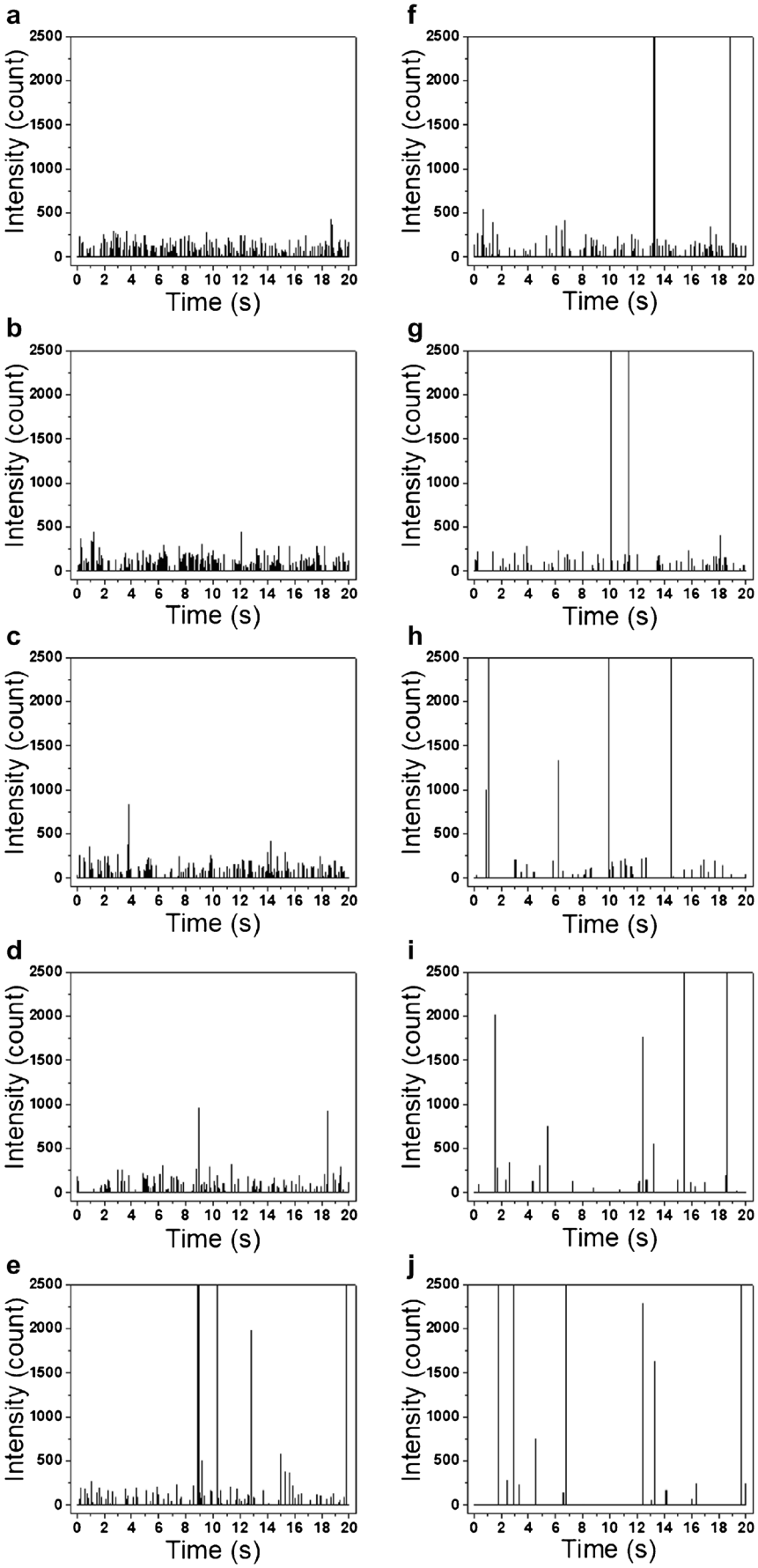

Fig. 3 spICP-MS measurements of AuNP-ssDNA in the presence of different concentrations of Hg^{2+}. **a**, without Hg^{2+}; **b**-**j**, Hg^{2+} concentrations in 0.01 ng L^{-1}, 0.1 ng L^{-1}, 1 ng L^{-1}, 10 ng L^{-1}, 100 ng L^{-1}, 1 μg L^{-1}, 10 μg L^{-1}, 100 μg L^{-1}, 1 mg L^{-1}. (^{197}Au, dwell time: 5 ms)

the change in particle number is much greater with aggregation (i.e., more sensitive) than the average measured intensity, especially at low Hg^{2+} concentrations, The assay conditions optimized using γ included concentration of AuNP-DNAs (optimum 10^8 P mL^{-1}), incubation temperature (optimum 30 °C), and incubation time (optimum 2 h). Respective data and figures are given in the Electronic Supporting Material (Figure S4).

Method characterization

Analytical performance of the optimized spICP-MS method was evaluated over a 10^8 range of Hg^{2+} concentrations; from 0.01 ng L^{-1} to 10 mg mL^{-1}. Raw spICP-MS measurements for only 20 s of the 180 s acquisition period are shown in Fig. 3. Observation of fewer particles overall but more nanoparticle clusters with higher Hg^{2+} concentration confirm the aggregation model proposed in Scheme 1. TEM images of the same samples (Fig. 4) also confirm more aggregation of AuNPs with higher mercury levels. Calibration plots of aggregation efficiency (γ) and average particle intensity versus Hg^{2+} concentration (Fig. 5, and Figure S5, respectively) also confirm these characteristics quantitatively. The average particle intensity increases significantly at high mercury levels, but the increase is accompanied by unacceptably large variations from sample-to-sample and changes at low mercury levels are too small to provide adequate sensitivity. Aggregation efficiency based on numbers of detected AuNP/clusters (γ) proved to be a far better quantitative metric for Hg^{2+} calibration and determination. It shows an extremely wide dynamic range

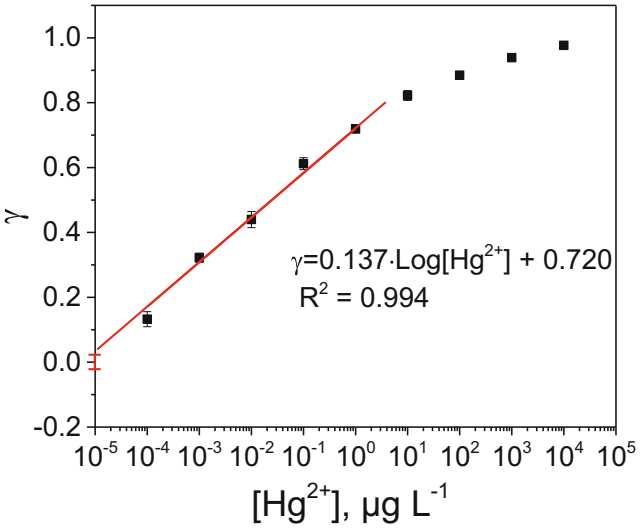

Fig. 5 Method calibration of aggregation efficiency (γ) with Hg^{2+} in concentration from 0.1 ng L^{-1} to 10 mg L^{-1}. Linear range from 0.1 ng L^{-1} to 1 μg L^{-1}. Optimized assay conditions included 10^8 P mL^{-1} concentration of AuNP-DNAs, 30 °C incubation temperature, and 2 h incubation time

covering almost the entire 10^8 range tested. The change in γ is reliably logarithmic between 0.1 to 1000 ng L^{-1} (line in Fig. 5, $\gamma = 0.137 \cdot \mathrm{Log}[Hg^{2+}] + 0.720$, R^2 0.994) making calibration straight forward and yielding an estimate of limit of detection (LOD = 0.031 ng L^{-1}, 155 fM) from three times the measured variance of aggregation efficiency ($\sigma = 0.021$) in the absence of mercury (i.e., when $\gamma = 0$). Overall, this method exhibits outstanding advantages in a linear range and detection limit compared to other AuNP aggregation or T-Hg^{2+}-T based strategies (Table 1).

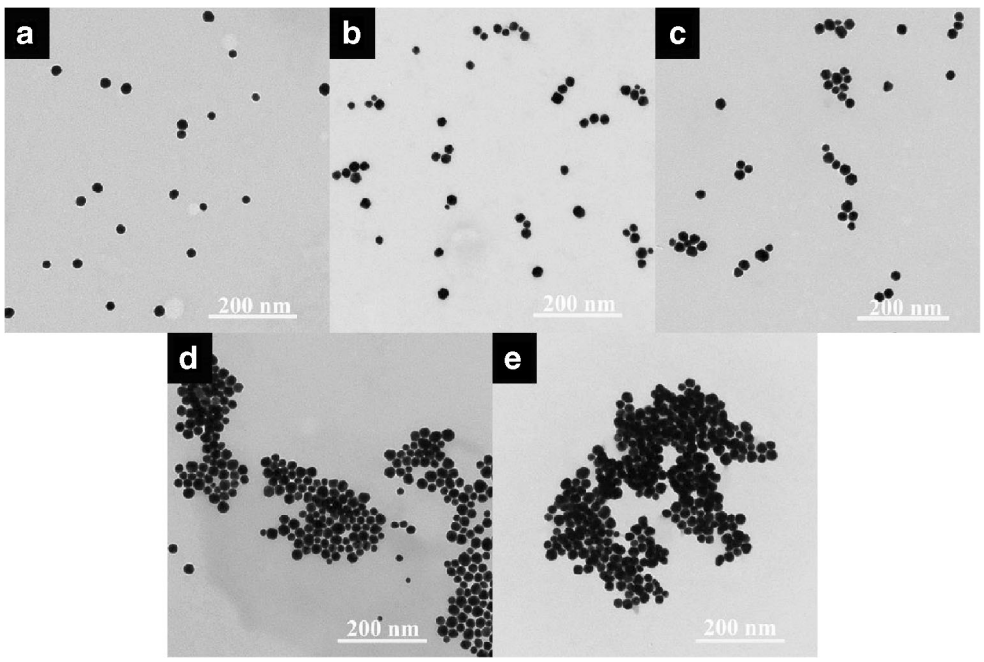

Fig. 4 TEM image of AuNP-ssDNA in the presence of different concentrations of Hg^{2+}. **a**, AuNP-ssDNA without Hg^{2+}; **b**-**e**, AuNP-ssDNA with Hg^{2+} in 10 μg L^{-1}, 100 μg L^{-1}, 1 mg L^{-1}, 10 mg L^{-1}

Table 1 Comparison of Hg^{2+} analysis methods based on AuNP aggregation or T-Hg^{2+}-T strategies

Methods	Materials	LOD	Linear range	Strategy	References
Colorimetric	AuNPs, APTES	10 nM	0–92.3 nM	Aggregation, APTES	[32]
Colorimetric	AuNPs, DNA	1 nM	1 nM-0.5 μM	Aggregation, NaCl	[23]
Colorimetric	AuNPs, CDs	7.5 nM	10–300 nM	Aggregation, CDs	[33]
Colorimetric (paper-based)	AuNPs, DNA	50 nM	25–100 nM	Aggregation, NaCl	[34]
Colorimetric & Fluorescence	AuNPs, DNA	0.1 nM	0.2–100 nM	Aggregation, NaCl	[35]
Colorimetric	AuNPs, DNA, Polymer	0.15 nM	0.25–500 nM	Aggregation, Polymer	[36]
Fluorescence	AuNPs, DNA	16 nM	0.02–1 μM	Quench, T-Hg^{2+}-T	[13]
Localized surface plasmon resonance	AuNPs, DNA	0.7 nM	1–50 nM	Aggregation, T-Hg^{2+}-T	[37]
Colorimetric	AuNPs, DNA	0.9 nM	1 nM-10 μM	Aggregation, T-Hg^{2+}-T	[38]
Fluorescence	Graphitic carbon nitride quantum dots	0.15 nM	1–500 nM	Quench, T-Hg^{2+}-T	[39]
Impedimetric	DNA	0.16 fM	1 fM-10 pM	T-Hg^{2+}-T	[40]
Voltammetric	Reduced graphene oxide@gold nanorods	0.24 nM	1–200 nM	T-Hg^{2+}-T	[41]
spICP-MS	AuNPs, DNA	0.031 ng L^{-1} (155 fM)	0.1 ng L^{-1} (500 fM)-1 μg L^{-1} (5 nM)	Aggregation, T-Hg^{2+}-T	This work

Method selectivity

To evaluate method selectivity for Hg^{2+}, AuNP-ssDNA mixtures containing 1 μg L^{-1} Hg^{2+} were separately incubated with other environmentally relevant di- and trivalent metal ions (Pb^{2+}, Cd^{2+}, Ni^{2+}, Mn^{2+}, Cu^{2+}, Fe^{2+}, Mg^{2+}, Zn^{2+}, Ca^{2+}, Al^{3+}, and Fe^{3+}) present a 100 μg L^{-1}. Despite the concentration of other ions being 100-fold higher, the results in Fig. 6 demonstrate that the AuNP-ssDNA probes aggregate very selectively with Hg^{2+} and none of the other ions showed an aggregation efficiency higher than 30% of that for Hg^{2+}.

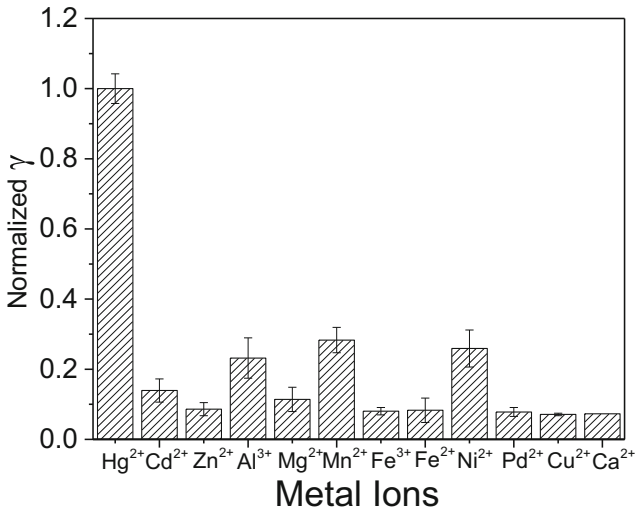

Fig. 6 Selectivity of the AuNP-ssDNA probe for Hg^{2+} determination by spICP-MS. Hg^{2+} concentration: 1 μg L^{-1}; other ion concentrations: 100 μg L^{-1}

Method validations and limitations

Recovery measurements for both tap water and river water samples were used to evaluate the optimized method for potential matrix interferences. Both sample types were spiked with varied levels of Hg^{2+} standards (1 ng L^{-1} and 1 μg L^{-1}) and the spICP-MS testing was performed in parallel with the standard EPA method 7473 (mercury by amalgamation/atomic absorption). The spike recovery results are compared (Table 2). Although the 1 ng L^{-1} spike level is below the detection limit of the EPA method, the results for the higher spike level (1 μg L^{-1}) show good correspondence and acceptable recoveries (100 ± 20%). The spICP-MS method also demonstrates acceptable Hg^{2+} recoveries at both concentration levels, even for the more complex river water matrix.

Accuracy of the optimized method was evaluated by triplicate analysis of the NIST certified reference material SRM1641e (Mercury in Water) after dilution to a linear portion of the calibration range (1 ng L^{-1}). The average Hg^{2+} concentration and 95% confidence interval ($N = 3$) obtained for the original sample was in agreement with the certified concentration (Table S3), indicating no apparent bias.

Although the method appears to be both accurate and robust for relatively simple water matrices, severe limitations in accuracy or linear range may occur with brines, solids and sludges. The high ionic strength associated with brines and acid-digested solid samples will likely interfere

Table 2 Comparison of Hg^{2+} spike recoveries measured by optimized spICP-MS assay and EPA method 7473 for tap water and river water samples ($n = 3$)

Samples	Spiked ($\mu g\ L^{-1}$)	Found spICP-MS ($\mu g\ L^{-1}$)	Recovery spICP-MS (%)	Found EPA 7473 ($\mu g\ L^{-1}$)	Recovery EPA 7473 (%)
Tap water (Grand Forks, ND)	1.00×10^{-3}	$(1.1 \pm 0.1) \times 10^{-3}$	110 ± 10	a	–
	1.00	0.9 ± 0.2	90 ± 20	1.16 ± 0.06	115 ± 6
River water (Red River of the North, Grand Forks, ND)	1.00×10^{-3}	$(1.1 \pm 0.2) \times 10^{-3}$	110 ± 20	a	–
	1.00	0.9 ± 0.1	90 ± 10	1.15 ± 0.01	112 ± 1

[a] The concentration of Hg^{2+} was too low to be detected by EPA Method 7473

with binding of Hg^{2+} to the AuNP-ssDNA or cause indiscriminate aggregation even in the absence of mercury. More work is needed to evaluate these effects, but insensitivity of the method up to as much as 1 M NaCl in the incubation medium (Figure S3) suggests that problems of high-ionic strength samples can be overcome by adjusting conditions. One possibility is the use of the ethylene glycol-terminated alkylthiol TOEG6 during the ssDNA modification, This co-reagent is known to stabilize AuNP-ssDNA aggregates at high ionic strength (up to 3 M NaCl) [30].

Conclusions

Ionic mercury (Hg^{2+}) in relatively simple aqueous samples has been successfully determined by using aggregation of DNA modified AuNPs and measurement of that aggregation by spICP-MS. Because of the strong and highly specific "T-Hg^{2+}-T" interactions between modified AuNPs, the method achieves outstanding sensitivity and selectivity. The optimized assay provides a 10^8 dynamic range, a broad and reliable logarithmic range from 0.1 ng L^{-1} to 1 μg L^{-1}, and a detection limit of 0.031 ng L^{-1} (155 fM). This assay also demonstrates accurate analysis of Hg^{2+} in certified reference material and satisfactory recovery from mercury-spiked tap water and river water matrices. These characteristics are superior to most other reported mercury assays and the method itself demonstrates a new spICP-MS strategy can provide for the detection of other metal ions or biomolecules by the careful design of the nanoparticle probes.

Acknowledgements This work was supported by the NSF grant CHE 1709160 (J.X.Z.), UND Applied Research to Address the State's Critical Needs Initiative program (X.W.) and the NIH grant 5P20GM103442-18 (D.T.P), The authors acknowledge the use of the Edward C. Carlson Imaging and Image Analysis Core Facility which is supported in part by NIH grant 1P20GM113123 and P20GM103442 and also acknowledge use of the North Dakota INBRE Metal Analysis Core Facility, which is supported in part by NIH grant 5P20GM103442-18.

Compliance with ethical standards

Conflict of interest The author(s) declare that they have no conflict of interest.

References

1. da Silva AD, Barbosa FJ, ScaranoWR (2012) Oral exposure to methylmercury modifies the prostatic microenvironment in adult rats. Int J Exp Pathol 93: 354–360
2. Schneider L, Peleja RP, Kluczkovski A, Freire GM, Marioni B, Vogt RC, Da Silveira R (2012) Mercury concentration in the spectacled caiman and black caiman (alligatoridae) of the amazon: implications for human health. Arch Environ Contam Toxicol 63: 270–279
3. Yu T, Zhang T-T, Zhao W, Xu J-J, Chen H-Y (2017) A colorimetric/fluorescent dual-mode sensor for ultra-sensitive detection of Hg^{2+}. Talanta 165:570–576
4. Rebelo FM, Caldas ED (2016) Arsenic, lead, mercury and cadmium: toxicity, levels in breast milk and the risks for breastfed infants. Environ Res 151:671–688
5. Lamborg CH, Hammerschmidt CR, Bowman KL, Swarr GJ, Munson KM, Ohnemus DC, Lam PJ, Heimbürger L-E, Rijkenberg MJA, Saito MA (2014) A global ocean inventory of anthropogenic mercury based on water column measurements. Nature 512:65
6. Farina M, Avila DS, da Rocha JBT, Aschner M (2013) Metals, oxidative stress and neurodegeneration: a focus on iron, manganese and mercury. Neurochem Int 62:575–594
7. Chen S, Liu D, Wang Z, Sun X, Cui D, Chen X (2013) Picomolar detection of mercuric ions by means of gold–silver core–shell nanorods. Nanoscale 5:6731–6735
8. Ou L, Chen C, Chen L, Wang H, Yang T, Xie H, Tong Y, Hu D, Zhang W, Wang X (2015) Low-level prenatal mercury exposure in North China: an exploratory study of anthropometric effects. Environ Sci Technol 49:6899–6908
9. Buck KA, Varian-Ramos CW, Cristol DA, Swaddle JP (2016) Blood mercury levels of zebra finches are heritable: implications for the evolution of mercury resistance. PLoS One 11:e0162440
10. Manna B, Raj CR (2018) Nanostructured sulfur-doped porous reduced graphene oxide for the ultrasensitive electrochemical detection and efficient removal of Hg(II). ACS Sustain Chem Eng 6: 6175–6182
11. Niece BK, Hauri JF (2013) Determination of mercury in fish: a low-cost implementation of cold-vapor atomic absorbance for the undergraduate environmental chemistry laboratory. J Chem Educ 90: 487–489
12. Bank MS (2012) Mercury in the environment: pattern and process. University of California Press, Berkeley

13. Tan D, He Y, Xing X, Zhao Y, Tang H, Pang D (2013) Aptamer functionalized gold nanoparticles based fluorescent probe for the detection of mercury (II) ion in aqueous solution. Talanta 113:26–30
14. Wang H, Wang Y, Jin J, Yang R (2008) Gold nanoparticle-based colorimetric and "turn-on" fluorescent probe for mercury(II) ions in aqueous solution. Anal Chem 80:9021–9028
15. Bagheri H, Naderi M (2009) Immersed single-drop microextraction–electrothermal vaporization atomic absorption spectroscopy for the trace determination of mercury in water samples. J Hazard Mater 165:353–358
16. Pierce DT, Zhao JX (2010) Trace analysis with Nanomaterials. Wiley, Weinheim
17. Saha K, Agasti SS, Kim C, Li X, Rotello VM (2012) Gold nanoparticles in chemical and biological sensing. Chem Rev 112:2739–2779
18. Daniel M-C, Astruc D (2004) Gold nanoparticles: assembly, supramolecular chemistry, quantum-size-related properties, and applications toward biology, catalysis, and nanotechnology. Chem Rev 104:293–346
19. Zeng S, Yong K-T, Roy I, Dinh X-Q, Yu X, Luan F (2011) A review on functionalized gold nanoparticles for biosensing applications. Plasmonics 6:491
20. Li RLJ (2004) Label-free colorimetric detection of specific sequences in genomic DNA amplified by the polymerase chain reaction. J Amer Chem Soc 126:10958–10961
21. Liu CW, Hsieh YT, Huang CC, Lin ZH, Chang HT (2008) Detection of mercury(II) based on Hg^{2+} -DNA complexes inducing the aggregation of gold nanoparticles. Chem Commun (Camb) 2242-2244
22. Du J, Zhu B, Chen X (2013) Urine for plasmonic nanoparticle-based colorimetric detection of mercury ion. Small 9:4104–4111
23. Li D, Wieckowska A, Willner I (2008) Optical analysis of Hg^{2+} ions by oligonucleotide-gold-nanoparticle hybrids and DNA-based machines. Angew Chem Int Ed Eng 47:3927–3931
24. Da Q, Gu Y, Peng X, Zhang L, Du S (2018) Colorimetric and visual detection of mercury(II) based on the suppression of the interaction of dithiothreitol with agar-stabilized silver-coated gold nanoparticles. Mikrochim Acta 185:357
25. Montano MD, Olesik JW, Barber AG, Challis K, Ranville JF (2016) Single particle ICP-MS: advances toward routine analysis of nanomaterials. Anal Bioanal Chem 408:5053–5074
26. Degueldre C, Favarger PY (2003) Colloid analysis by single particle inductively coupled plasma-mass spectroscopy: a feasibility study. Colloids and Surf A: Physicochem Eng Asp 217:137–142
27. Laborda F, Bolea E, Jimenez-Lamana J (2014) Single particle inductively coupled plasma mass spectrometry: a powerful tool for nanoanalysis. Anal Chem 86:2270–2278
28. Mohini M, Kapil K, Durgadas A, Ravindra KR (2017) ICP-MS: analytical method for identification and detection of elemental impurities. Curr Drug Discov Technol 14:106–120
29. Han G, Xing Z, Dong Y, Zhang S, Zhang X (2011) One-step homogeneous DNA assay with single-nanoparticle detection. Angew Chem Int Ed Eng 50:3462–3465
30. Deka J, Mech R, Ianeselli L, Amenitsch H, Cacho-Nerin F, Parisse P, Casalis L (2015) Surface passivation improves the synthesis of highly stable and specific DNA-functionalized gold nanoparticles with variable DNA density. ACS Appl Mater Interfaces 7:7033–7040
31. Li M, Zhou X, Ding W, Guo S, Wu N (2013) Fluorescent aptamer-functionalized graphene oxide biosensor for label-free detection of mercury(II). Biosens Bioelectron 41:889–893
32. Xie Y (2018) Colorimetric determination of Hg(II) via the gold amalgam induced deaggregation of gold nanoparticles. Mikrochim Acta 185:351
33. Wang F, Sun J, Lu Y, Zhang X, Song P, Liu Y (2018) Dispersion-aggregation-dispersion colorimetric detection for mercury ions based on an assembly of gold nanoparticles and carbon nanodots. Analyst 143:4741–4746
34. Chen GH, Chen WY, Yen YC, Wang CW, Chang HT, Chen CF (2014) Detection of mercury(ii) ions using colorimetric gold nanoparticles on paper-based analytical devices. Anal Chem 86:6843–6849
35. Yang L, Yun W, Chen Y, Wu H, Liu X, Fu M, Huang Y (2017) Ultrasensitive colorimetric and fluorometric detection of Hg(II) based on the use of gold nanoparticles and a catalytic hairpin assembly. Microchim Acta 184:4741–4747
36. Zhu Y, Cai Y, Zhu Y, Zheng L, Ding J, Quan Y, Wang L, Qi B (2015) Highly sensitive colorimetric sensor for Hg(2+) detection based on cationic polymer/DNA interaction. Biosens Bioelectron 69:174–178
37. Jia S, Bian C, Sun J, Tong J, Xia S (2018) A wavelength-modulated localized surface plasmon resonance (lspr) optical fiber sensor for sensitive detection of mercury(ii) ion by gold nanoparticles-DNA conjugates. Biosens Bioelectron 114:15–21
38. Song X, Wang Y, Liu S, Zhang X, Wang H, Wang J, Huang J (2019) Colorimetric and visual mercury(ii) assay based on target-induced cyclic enzymatic amplification, thymine-Hg(II)-thymine interaction, and aggregation of gold nanoparticles. Mikrochim Acta 186:105
39. Achadu OJ, Revaprasadu N (2018) Microwave-assisted synthesis of thymine-functionalized graphitic carbon nitride quantum dots as a fluorescent nanoprobe for mercury(II). Mikrochim Acta 185:461
40. Gao F, Zhang T, Chu Y, Wang Q, Song J, Qiu W, Lin Z (2018) Ultrasensitive impedimetric mercury(II) sensor based on thymine-Hg(II)-thymine interaction and subsequent disintegration of multiple sandwich-structured DNA chains. Mikrochim Acta 185:555
41. Jin H, Zhang M, Wei M, Cheng JH (2019) A voltammetric biosensor for mercury(II) using reduced graphene oxide@gold nanorods and thymine-Hg(II)-thymine interaction. Mikrochim Acta 186:264